© 2014. Published by The Company of Biologists Ltd | Journal of Cell Science (2014) 127, 1476–1486 doi:10.1242/jcs.138495

RESEARCH ARTICLE

sept7b is essential for pronephric function and development of left–right asymmetry in zebrafish embryogenesis

Surjya Narayan Dash[1], Eero Lehtonen[1,2], Anita A. Wasik[1], Antonino Schepis[3], Jere Paavola[4], Pertti Panula[5], W. James Nelson[3] and Sanna Lehtonen[1,*]

ABSTRACT

The conserved septin family of filamentous small GTPases plays important roles in mitosis, cell migration and cell morphogenesis by forming scaffolds and diffusion barriers. Recent studies in cultured cells *in vitro* indicate that a septin complex of septin 2, 7 and 9 is required for ciliogenesis and cilia function, but septin function in ciliogenesis in vertebrate organs *in vivo* is not understood. We show that *sept7b* is expressed in ciliated cells in different tissues during early zebrafish development. Knockdown of *sept7b* by using morpholino antisense oligonucleotides caused misorientation of basal bodies and cilia, reduction of apical actin and the shortening of motile cilia in Kupffer's vesicle and pronephric tubules. This resulted in pericardial and yolk sac edema, body axis curvature and hydrocephaly. Notably, in *sept7b* morphants we detected strong left–right asymmetry defects in the heart and lateral plate mesoderm (*situs inversus*), reduced fluid flow in the kidney, the formation of kidney cysts and loss of glomerular filtration barrier function. Thus, *sept7b* is essential during zebrafish development for pronephric function and ciliogenesis, and loss of expression of *sept7b* results in defects that resemble human ciliopathies.

KEY WORDS: Kidney, Cilia, Septin 7, *sept7b*, Rab8, Ciliogenesis, Vesicle trafficking

INTRODUCTION

Septins are a highly conserved family of GTP-binding proteins that polymerize into heteromeric filaments (Joberty et al., 2001; Nagata et al., 2004) that associate with the actin (Kinoshita et al., 2002; Kinoshita et al., 1997) and microtubule cytoskeletons (Bowen et al., 2011; Sakamoto et al., 2008). Septins were originally discovered in a screen for temperature-sensitive cell division mutants in yeast (Hartwell, 1971). There are 14 septin genes in humans (Hall et al., 2005; Peterson et al., 2007), which play roles in mitosis (Spiliotis et al., 2005), vesicle trafficking (Beites et al., 1999; Spiliotis et al., 2008) and membrane compartmentalization in specialized structures – such as the primary cilium (Hu et al., 2010; Kim et al., 2010).

[1]University of Helsinki, Haartman Institute, Department of Pathology, Haartmaninkatu 3, 00290 Helsinki, Finland. [2]University of Helsinki, Laboratory Animal Center, Haartmaninkatu 3, 00290 Helsinki, Finland. [3]Department of Biology, The James H. Clark Center, Stanford University, 318 Campus Drive, Stanford, CA 94305-5435, USA. [4]Minerva Institute for Medical Research, Biomedicum 2U, Tukholmankatu 8, 00290 Helsinki, Finland. [5]University of Helsinki, Neuroscience Center and Institute of Biomedicine/Anatomy, Haartmaninkatu 8, 00290 Helsinki, Finland.

*Author for correspondence (sanna.h.lehtonen@helsinki.fi)

Received 16 July 2013; Accepted 8 January 2014

Septin filaments comprise three different septin proteins (Joberty et al., 2001; Nagata et al., 2004). Septin 2, 6 and 7 have been reconstituted into filaments, and the filament structure has been solved by X-ray crystallography (Sirajuddin et al., 2007). Septin 2 and 7 localize at the base of the primary cilium of epithelial cells in tissue culture and *Xenopus* epidermis, and expression of the complex is required for ciliogenesis (Ghossoub et al., 2013; Hu et al., 2010; Kim et al., 2010) and as a ciliary membrane protein diffusion barrier (Chih et al., 2011; Hu et al., 2010). Septin 7 is expressed in glomerular epithelial cells (podocytes) in mouse and rat, and regulates glucose transporter trafficking in cultured podocytes (Wasik et al., 2012). Septin 7 interacts with nephrin and CD2-associated protein (CD2AP) (Wasik et al., 2012), both of which are expressed in podocytes and are essential for kidney ultrafiltration function (Kestilä et al., 1998; Shih et al., 1999). In cultured hippocampal neurons, septin 7 regulates dendritic branching and the morphology of dendritic spines during neuronal maturation (Hu et al., 2012; Tada et al., 2007; Xie et al., 2007). Despite the apparent importance of the expression of septin 7 in various cell types, little is known about its function *in vivo*.

Zebrafish is an excellent model for developmental and genetic studies, and for studying conserved mechanisms underlying human diseases, such as in the kidney. The zebrafish pronephric kidney has two nephrons with fused glomeruli and pronephric tubules that fuse before reaching the cloaca, and it comprises the same cell types as the nephrons of other vertebrates (Drummond et al., 1998). Previous studies have indicated that several kidney defects in zebrafish are associated with abnormal fluid flow that leads to the accumulation of fluid in the body (Ebarasi et al., 2011; Kramer-Zucker et al., 2005a). An important cause of fluid accumulation is cilia dysfunction.

Cilia are highly conserved organelles that play an important role in motility, sensory functions and signaling events (Bisgrove and Yost, 2006). The cilia in cultured mouse kidney epithelial cells act as sensors of mechanical signals that are created by fluid flow and transduce the signals into an intracellular Ca^{2+} response (Nauli et al., 2003). Mutations in ciliary proteins lead to cystic diseases, termed ciliopathies, that affect the kidneys and other ciliated organs (Bisgrove and Yost, 2006). In zebrafish, changes in motile cilia structure, function or number can lead to disruption of fluid flow in the pronephros, brain and Kupffer's vesicle, which can result in cyst formation (Kramer-Zucker et al., 2005a).

Dysfunction of the mammalian septin family has been identified in diverse pathologies, including neoplasia (Montagna et al., 2003), neurodegenerative conditions (Kinoshita et al., 1998) and infections (Kim et al., 2007). However, the function of septins in the kidney *in vivo* has not been studied; such analysis is required to test the relevance of the functions of septins in ciliogenesis and cilia structure that have been identified in epithelial cells in tissue culture. There are two paralogous septin 7 genes in zebrafish, *sept7a* and *sept7b*, and

Journal of Cell Science

Journal of Cell Science (2014) 127, 1476–1486 doi:10.1242/jcs.138495

we have reported previously that septin 7 is expressed in kidney epithelial cells in mammals (Wasik et al., 2012). Here, we show that knockdown of *sept7b* in zebrafish results in specific developmental defects, indicating that *sept7a* does not functionally compensate for *sept7b*. We show that *sept7b* is expressed in the pronephros and other ciliated cell types, and that *sept7b* depletion causes misorientation of basal bodies and cilia. These defects reduce fluid flow, disrupt the glomerular filtration barrier, cause cyst formation in the pronephros, hydrocephaly and defects in the left–right asymmetry. These results indicate that *sept7b* plays an important role in the structural and functional organization of the pronephros, and a general role in regulating the structure and function of motile and non-motile cilia. Notably, loss of *sept7b* expression gives rise to multiple developmental defects that are similar to human ciliopathies.

RESULTS

sept7b is expressed in the brain and pronephros in developing zebrafish

We cloned the zebrafish orthologue of mammalian septin 7, *sept7b* (supplementary material Fig. S1), and first studied its distribution by detecting its mRNA and protein in developing zebrafish embryos. Quantitative real-time PCR (qRT-PCR) showed that *sept7b* expression was high in fertilized embryos at 0 hours post fertilization (hpf) and persisted during the larval stages (Fig. 1A). *sept7b* mRNA was detected by whole-mount *in situ* hybridization in 3-hpf embryos (Fig. 1B) and was widely expressed in larvae at 4 days post fertilization (dpf) and concentrated in the brain and pronephros (Fig. 1C,E); no signal was detected with the sense probe (Fig. 1D,F). To confirm that *sept7b* is expressed in the pronephros, we performed histological analysis of *in situ* hybridized 2-dpf embryos that revealed expression of *sept7b* in the pronephric tubules and the glomerulus (Fig. 1G). To analyze the localization of the septin 7 protein in the pronephros, we performed immunostaining of frozen sections of 4-dpf *wt1b::GFP* larvae, which revealed that septin 7 was concentrated in pronephric tubule cells (Fig. 1H,I) and in glomerular podocytes (Fig. 1J,K). These results are in accordance with our previous results showing that septin 7 is expressed in podocytes and tubules in the rat kidney (Wasik et al., 2012), and that expression of septin 7 is conserved in different vertebrates.

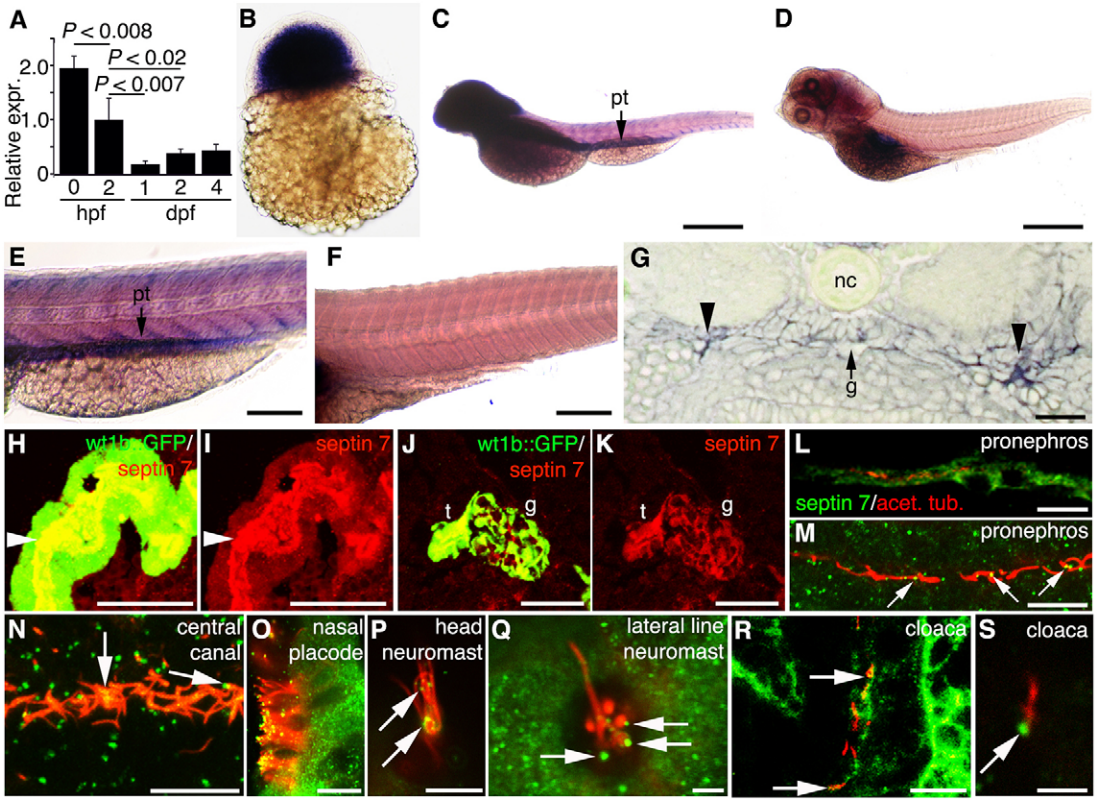

Fig. 1. Septin 7 is expressed throughout zebrafish development and is enriched in the brain and pronephros. *sept7b* mRNA expression in zebrafish larvae (A–E). (A) By using qRT-PCR and normalizing to *rps3* (ribosomal protein subunit 3), it can be seen that *sept7b* is expressed in fertilized embryos at 0 hpf, 2 hpf and in 1–4-dpf embryos and larvae. (B) *In situ* hybridization shows that *sept7b* is expressed in 3-hpf embryos. (C–F) Lateral views of 4-dpf larvae hybridized with *sept7b* antisense (C,E) and sense (D,F) probes. (C,E) *sept7b* mRNA is concentrated in the brain and the pronephric tubule (pt). (D,F) The sense probe shows no signal, except in the swim bladder region (D). (G) A section of a 2-dpf embryo shows *sept7b* mRNA in the glomerulus (arrow labeled g) and the pronephric tubule (arrowheads). Notochord, nc. (H–K) The septin 7 protein is localized in the pronephric tubule and glomerulus. (H,I) Immunostaining shows that septin 7 (red) localizes in the pronephric tubule cells (t; arrowhead), and in the glomerulus (g) of 4-dpf *wt1b::GFP* zebrafish larvae (J,K). (L–S) Septin 7 is expressed in ciliated cells in 72-hpf embryos. Cilia are visualized by staining for acetylated tubulin (red). Septin is indicated by green fluorescence. (L) Septin 7 localizes in pronephric tubule cells. (M) In addition to localizing in the cytoplasm of pronephric tubule cells, septin 7 concentrates at the base of or along the cilia (arrows). (N) Septin 7 is found at the base of, or along, the cilia in the central canal (arrows). (O) Septin 7 is expressed in nasal epithelial cells, along the ciliary axoneme and in the tips of cilia. (P) Septin 7 is localized along the axoneme of the neuromast in the head region (arrows). (Q) In lateral line neuromasts, septin 7 is found close to the base of cilia (arrows). (R) In the cloaca region, septin 7 is found in the epithelium and at the base of cilia (arrows). (S) Higher magnification reveals a concentration of septin 7 at the base of cilia in cloaca (arrow). Scale bars: 100 µm (B,E,F); 300 µm (C,D); 20 µm (G,R); 50 µm (H,I); 40 µm (J,K); 10 µm (L–O); 7.5 µm (P); 2.5 µm (Q); 3 µm (S).

Journal of Cell Science

Journal of Cell Science (2014) 127, 1476–1486 doi:10.1242/jcs.138495

Septin 7 protein is expressed in ciliated epithelia

To investigate the subcellular localization of septin 7 in zebrafish, we used confocal microscopy to image septin 7 and acetylated tubulin (Fig. 1L–S). Septin 7 was localized in the cytoplasm of pronephric tubule cells, and concentrated at the base and along pronephric cilia (Fig. 1L,M). Septin 7 was also localized at the base of and along the cilia in the central canal of the spinal cord (Fig. 1N). In the nasal placode, septin 7 was observed both in the cytoplasm of the epithelial cells and along the cilium (Fig. 1O). In neuromasts in the head region (Fig. 1P) and the lateral line (Fig. 1Q), septin 7 was observed at the base and along the cilia, and in the cloaca region septin 7 was prominent in the epithelial cells and at the base of cilia (Fig. 1R,S). These data indicate that septin 7 is predominantly expressed in the pronephros and in ciliated cells in a variety of organs.

Suppression of *sept7b* induces pronephric cysts and pericardial and yolk sac edema

To study the function of *sept7b*, we injected embryos with two types of morpholino antisense oligonucleotides; one causes a splicing defect of *sept7b* targeting exon 2 (splice-blocking morpholino antisense oligonucleotide targeting exon 2, SBMO-2), and the other blocks the initiation of translation of *sept7b* (translation-blocking morpholino antisense oligonucleotide, TBMO). The splicing defect caused by SBMO-2 was confirmed by using PCR, which revealed a smaller amplicon in the morphant compared with the control (Fig. 2A), and sequencing showed that exon 2 was skipped. The effect of the TBMO in blocking the translation of *sept7b* was confirmed by western blotting, which showed that the expression level of septin 7 was reduced by 84% and 73% compared with controls in 2- and 4-dpf morphants, respectively (Fig. 2B). At 2 and 4 dpf, in embryos that had been injected with SBMO-2, qRT-PCR further confirmed that the *sept7b* mRNA was reduced by 89% and 92%, respectively (Fig. 2C).

We identified several prominent phenotypic defects in the *sept7b* TBMO morphants (Fig. 2E–H). The 3-dpf morphants exhibited pronephric cysts and pericardial edema (Fig. 2F), whereas embryos injected with the TBMO-MM (TBMO-mismatch) did not display an altered phenotype (Fig. 2E). At 4 dpf, 80% of the morphants that had been injected with the *sept7b* TBMO exhibited pronephric cysts that had enlarged to pronephric dilations. In addition, pericardial and yolk sac edema, and hydrocephaly were observed in 91% of larvae, and body axis curvature was observed in 41% of larvae (Fig. 2H; $n=200$). SBMO-2-injected embryos had a similar phenotype at 4 dpf (Fig. 2I; $n=200$) to morphants injected with the *sept7b* TBMO but, because only 11% of larvae injected with the SBMO-2 had phenotypic defects, we used the TBMO throughout the remainder of the study.

To rescue defects associated with knockdown of *sept7b*, we co-injected capped *sept7b* mRNA with *sept7b* MOs (Fig. 2D,J). qRT-PCR showed a slightly lower level of *sept7b* mRNA expression in embryos that had been rescued, by co-injecting the embryos with capped *sept7b* mRNA and the SBMO-2, compared with the control (Fig. 2D). However, this amount of capped *sept7b* mRNA was sufficient to restore the function of *sept7b* because pericardial edema and hydrocephalus were found in 9% of embryos, and a curved body was found in 10% of embryos co-injected with the TBMO and *sept7b* capped mRNA ($n=200$). Pericardial edema and hydrocephalus were found in 3.5% of embryos and a curved body was found in 5% of embryos co-injected with the SBMO-2 and *sept7b* capped mRNA ($n=200$). The phenotype of 4-dpf larvae co-injected with the *sept7b* TBMO and capped *sept7b* mRNA (Fig. 2J) was similar to the phenotype of 4-dpf larvae that had been injected with the TBMO-MM control (Fig. 2G). To confirm further the specificity of the *sept7b* MOs, we co-injected embryos with morpholino antisense oligonucleotides against p53 and *sept7b* that resulted in the persistence of abnormal phenotypes (data not shown), which further confirms the specificity of the defects that are induced by *sept7b* MOs.

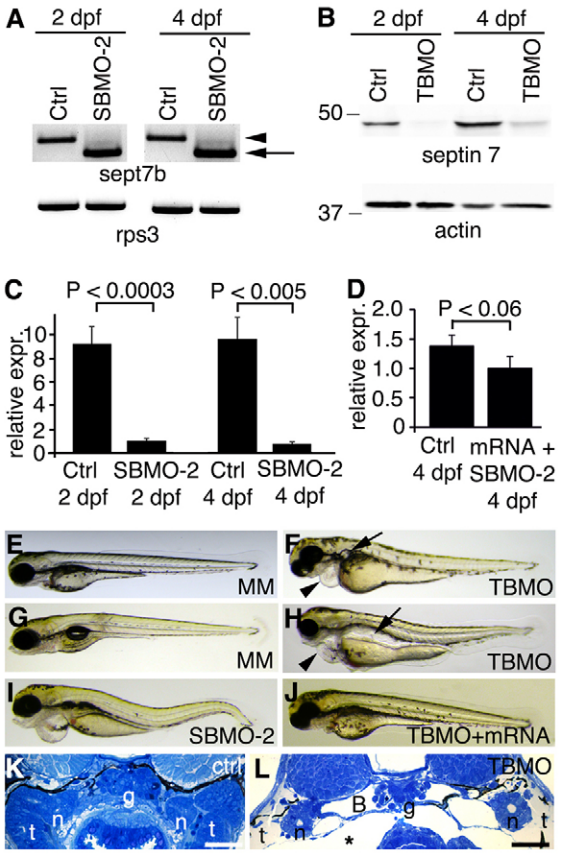

Fig. 2. *sept7b* knockdown causes body curvature, edema and pronephric cysts. (A) PCR confirms skipping of exon 2 (arrow; amplicon 626 bp) of *sept7b* in SBMO-2-injected embryos at 2 and 4 dpf. Arrowhead marks the non-spliced *sept7b* amplicon (726 bp). *Rps3* is used as a control (amplicon 428 bp). Ctrl, control. (B) Immunoblotting of 2- and 4-dpf larvae that had been injected with TBMO indicates that TBMO efficiently blocked translation of *sept7b* mRNA. Actin is used as a loading control. (C) qRT-PCR indicates that the expression level of *sept7b* is reduced by 89–92% in SBMO-2-injected embryos at 2 and 4 dpf. *Rps3* was used to normalize expression values. (D) qRT-PCR of 4-dpf larvae shows that the expression level of *sept7b* is partially restored in rescue experiments when capped zebrafish *sept7b* mRNA is co-injected with the *sept7b* SBMO-2. (E,F) Injection of the *sept7b* TBMO into embryos causes pericardial (arrowhead) and yolk sac edema, and pronephric cysts (arrow) at 3 dpf (F), whereas the TBMO-MM-injected embryos (MM) do not show phenotypic differences (E). (G,H) *sept7b* TBMO-injected larvae (H) show pericardial (arrowhead) and yolk sac edema, body axis curvature, and dilation of pronephric tubules (arrow) compared to the TBMO-MM-injected larvae at 4 dpf. (I) *sept7b* SBMO-2 injection causes pericardial edema and body axis curvature. (J) The phenotypic differences can be rescued by co-injection of *sept7b* capped mRNA with the *sept7b* TBMO. (K) Histological section of a 4-dpf control larvae. (L) *sept7b* morphant larvae at 4 dpf shows a dilated Bowman's space (B). g, glomerulus; n, neck segment of the pronephric tubule; t, pronephric tubule; asterisk, edema. Scale bars: 50 μm.

Journal of Cell Science

Journal of Cell Science (2014) 127, 1476–1486 doi:10.1242/jcs.138495

Knockdown of *sept7b* results in defects in podocyte and pronephric tubule morphology

S*ept7b* morphants had severe pericardial and yolk sac edema (Fig. 2F,H,I), indicating that *sept7b* plays a role in pronephric function. Histological examination of *sept7b* morphants at 4 dpf revealed that the Bowman's space had widened and edema had developed compared with controls (Fig. 2K,L). Analysis of the pronephros in control larvae, by using electron microscopy, revealed fine podocyte foot processes and slit diaphragms (Fig. 3A), whereas *sept7b* morphants typically showed effacement of podocyte foot processes, lack of slit diaphragms and, occasionally, extension of irregular microvillar-type cell processes from the apical surface of podocytes (Fig. 3B,C). In addition, the pronephric tubules of *sept7b* morphants were dramatically dilated compared with controls and showed sparser, irregular microvilli (Fig. 3D,E). However, the characteristic organization of microtubules in the cross-sections of cilia taken from *sept7b* morphant pronephric tubules appeared normal (Fig. 3F,G).

sept7b knockdown disrupts the glomerular filtration barrier and reduces fluid flow

Edema and enlargement of pronephric tubules in *sept7b* morphants indicate a defect in the function of the pronephros. This could be due to a disruption of the glomerular filtration function, as indicated by morphological alterations in the podocytes (Fig. 3B,C). To study the integrity of the glomerular filtration barrier, we injected 500-kDa fluorescein dextran into the pericardinal vein of 3.5-dpf TBMO-MM control and *sept7b*-TBMO-injected larvae ($n=20$ each), and analyzed whether the dye passed through the glomerular barrier. In controls, 500-kDa dextran was retained in the circulation, indicating that the glomerular filtration barrier was intact (Fig. 4A). However, in *sept7b* morphants, 500-kDa dextran passed through the glomerular barrier and was partially endocytosed in the pronephric tubule, indicating that the barrier function of the glomerulus was disrupted (Fig. 4B). We found that 10-kDa fluorescein dextran, which readily passes through the filtration barrier, was partially taken up in the tubules of both TBMO-MM control and *sept7b*-TBMO-injected larvae (Fig. 4C,D).

The disruption of pronephric function in *sept7b* morphants could be due to a ciliary defect that results in reduced fluid flow in pronephric tubules. To examine whether fluid flow is abnormal in *sept7b* morphants, we injected 70-kDa tetramethylrhodamine dextran, through the pericardium, into 53-hpf embryos ($n=24$) and examined the presence of dye within 20 min of injection (Fig. 4E,F) and again 24 h later (Fig. 4G,H). We found that the dye was cleared from the body in controls at 77 hpf (Fig. 4G) but was retained in *sept7b* morphants, indicating that the fluid flow was disrupted (Fig. 4H). To examine whether reduced clearance of dye was due to reduced cardiac function in the *sept7b* morphants, we measured the heart rate of control and morphant zebrafish. We did not find a significant difference in the heart rate at the time of dye injection (mean±s.d.; control, 106±3 beats/min; morphant, 106±3 beats/min; $n=10$ for each) or after 24 h (control, 110±2 beats/min; morphant, 101±1 beats/min; $n=10$ for each). Collectively, these results indicate that *sept7b* knockdown leads to defects in both the function of the glomerular barrier and tubular fluid flow, which manifests as reduced kidney function.

sept7b knockdown affects the length of cilia in pronephric epithelial cells and Kupffer's vesicle

At 30 hpf, we examined the length of cilia in the pronephros of *wt1b::GFP* embryos, which express GFP specifically in pronephric regions, that had been injected with the *sept7b* TBMO by staining for acetylated tubulin, a marker for cilia (Fig. 5A,B). The length of pronephric cilia was reduced from 10.88±0.91 µm in controls to 3.91±0.81 µm in *sept7b* morphants (mean±s.d.) (Fig. 5C). A similar defect in cilia length was observed in Kupffer's vesicle cilia, which are responsible for creating directional fluid flow (Essner et al., 2005). Staining of control and *sept7b* morphant embryos at 12–13 hpf (6–7-somite stage) for acetylated tubulin indicated that the length of Kupffer's vesicle cilia was reduced from 5.66±0.79 µm

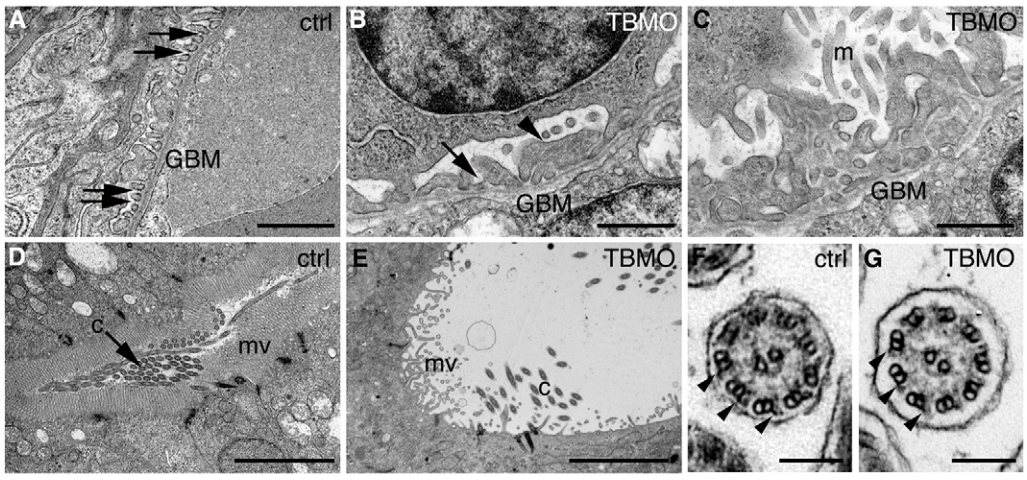

Fig. 3. Depletion of *sept7b* causes defects in the structure of the pronephros. (A—E) Electron micrographs of control and *sept7b*-morphant kidneys at 4 dpf. (A) Wild-type podocytes show regular foot processes connected by slit diaphragms (arrows). Glomerular basement membrane, GBM. (B,C) Podocytes of a s*ept7b* morphant (TBMO) show foot process effacement (arrowhead) and microvillar-type cell processes (m) on their apical surface. Occasional slit diaphragms (arrow) were observed. (D) A pronephric tubule of the wild-type larva (ctrl) shows regular microvilli (mv) and cilia (c) morphology. (E) A tubule in a s*ept7b* morphant appears dilated and shows sparse and irregular microvilli and scattered cilia. (F,G) The cilia in both control (F) and TBMO morphants (G) show the normal 9+2 structure of microtubules. The outer dynein arms are visible in both the control and *sept7b* morphant cilia (arrowheads). Scale bars: 1 µm (A–C); 10 µm (D,E); 140 nm (F,G).

Journal of Cell Science

Journal of Cell Science (2014) 127, 1476–1486 doi:10.1242/jcs.138495

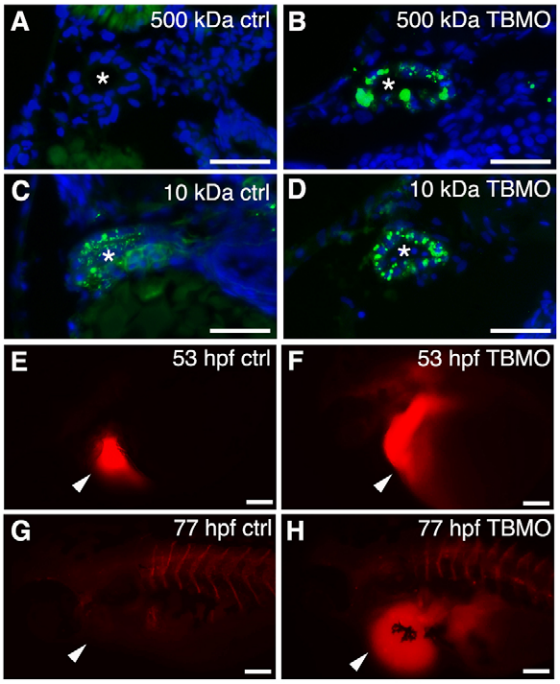

Fig. 4. Knockdown of *sept7b* affects glomerular barrier function and fluid flow. (A,B) 500--kDa fluorescein dextran (green) injected into the cardinal vein of 3.5-dpf larvae passes the glomerular barrier and is endocytosed into the pronephric tubules of *sept7b*-TBMO-injected larvae (B), whereas in the control (ctrl; A) the dextran remains in circulation. (C,D) 10-kDa fluorescein dextran readily passes the glomerular barrier in both control (C) and TBMO-injected (D) larvae and is endocytosed into the pronephric tubules. DAPI (blue) stains the nuclei, and the asterisk marks the lumen of the tubule. (E–H) Tetramethylrhodamine dextran (70,000-kDa) was injected into the pericardial sac (arrowheads) of control (E) or *sept7b*-TBMO-injected (F) embryos at 53 hpf that were imaged immediately after dye injection (E,F) and again at 77 hpf (G,H). Clearance of the dye was observed in the control larvae (G) but not in *sept7b* morphants (H). Scale bars: 20 μm (A–D); 200 μm (E–H).

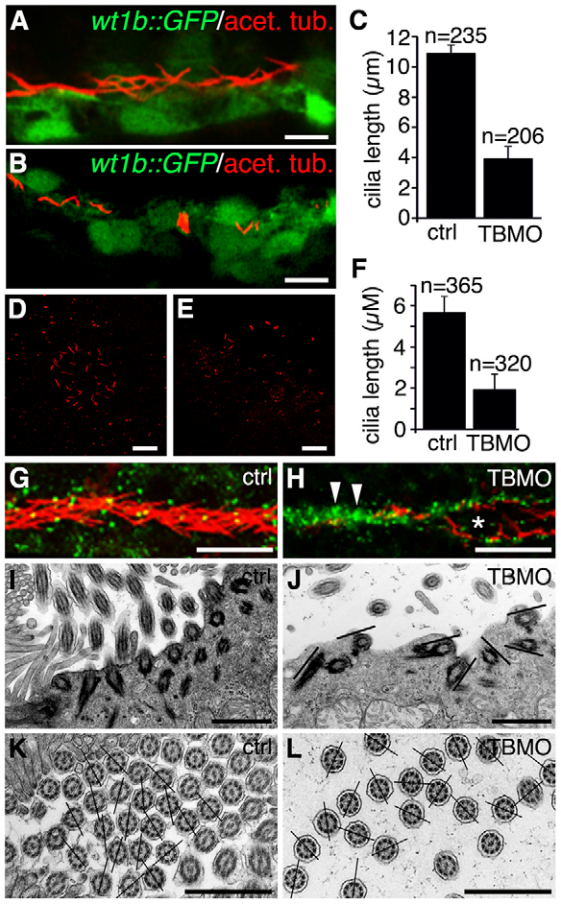

Fig. 5. Depletion of *sept7b* reduces the length of cilia in the pronephric tubule and Kupffer's vesicle, and causes misorientation of basal bodies and cilia. (A) Acetylated tubulin (red) stains cilia in 30-hpf *wt1b::GFP* embryos. (B) Staining of 30-hpf *sept7b*-TBMO morphants for acetylated tubulin (red) reveals shortened cilia, indicating that *sept7b* is essential for ciliogenesis. (C) The length of pronephric cilia is reduced in *sept7b* morphants (TBMO). Ctrl, control. (D,E) Kupffer's vesicle of control (D) and *sept7b* morphant (E) embryos at 12–13 hpf that have been stained for acetylated tubulin to visualize cilia. (F) The length of cilia of Kupffer's vesicle is reduced in *sept7b* morphants compared with controls. (G) Immunostaining of cilia for acetylated α-tubulin (red) and of basal bodies for γ-tubulin (green) in the multi-ciliated region of the pronephric tubule at 30 hpf in control embryos shows well-organized basal bodies that localized at the base of cilia in the tubular epithelial cells. (H) In *sept7b*-TBMO-injected embryos, the basal bodies are disorganized (arrowheads), the tubule diameter is increased (asterisk) and cilia appear misoriented. (I) Electron microscopy reveals apically docked basal bodies with outgrowths of ciliary axonemes in 4-dpf control larvae. (J) In *sept7b*-TBMO-injected larvae, the basal bodies docked at the apical cell membrane but appeared disorganized (indicated by the lines showing the orientation of the basal bodies). (K,L) The ciliary angle in control (20.9°; K) and *sept7b*-TBMO-injected larvae (41.1°; L) differed substantially, indicating that cilia are misoriented in *sept7b*-depleted larvae. The lines are drawn through the central pairs of the microtubules to indicate the orientation of the cilia. Scale bars: 20 μm (A,B,D,E,G,H); 1 μm (I–L).

in controls to 1.92±0.75 μm in *sept7b* morphants (Fig. 5D–F). In addition, the photoreceptor outer segments, which are specialized primary cilia, appeared shorter in *sept7b*-TBMO-injected zebrafish compared with controls (supplementary material Fig. S2).

To confirm further that septin 7 is required for cilia formation, we used mouse inner medullary collecting duct (mMICD3) cells. Septin 7 localized at the base of the primary cilium in mIMCD3 cells when ciliogenesis was induced by serum starvation (supplementary material Fig. S3A). Knockdown of septin 7 expression by using siRNA (supplementary material Fig. S3B–E) led to reduced numbers of ciliated cells (supplementary material Fig. S3F), and the length of cilia was reduced from 8.86±0.63 μm in cells transfected with control siRNA to 3.69±0.47 μm in cells transfected with siRNA against septin 7 (supplementary material Fig. S3G). Thus, septin 7 is required for ciliogenesis in epithelial cells *in vivo* and *in vitro*.

Depletion of *sept7b* causes misorientation of basal bodies and cilia in the pronephros

We investigated the organization and orientation of basal bodies and cilia in pronephric tubules. Double labeling with antibodies against acetylated tubulin and γ-tubulin, to visualize cilia and basal bodies, respectively, revealed that basal bodies aligned apically in an organized fashion in multi-ciliated pronephric tubule cells in control embryos (Fig. 5G). By contrast, in *sept7b* morphants the basal bodies were clustered and the cilia appeared misoriented in dilated tubules (Fig. 5H). By using electron microscopy, analysis of multi-ciliated pronephric tubule cells from *sept7b* morphants showed that basal bodies were docked at the apical cell surface but were misoriented (Fig. 5I,J). Note that the *sept7b* morpholino antisense oligonucleotide did not fully deplete the septin 7 protein, which might explain why some cilia

Journal of Cell Science

Journal of Cell Science (2014) 127, 1476–1486 doi:10.1242/jcs.138495

developed, although they were substantially shorter than controls, and the migration and docking of the basal bodies was not completely prevented.

We also analyzed the orientation of pronephric cilia using a technique that has been used in human patients with secondary or primary ciliary dyskinesia (De Iongh and Rutland, 1989; Jorissen and Willems, 2004). In this method, the angle between the lines defined by the central microtubules and a reference line is used to measure the orientation of cilia. The mean ciliary angle was 21.0° (s.d. 15.0) in controls compared with 41.1° (s.d. 25.9) in *sept7b* morphants ($n=148$ for each) (Fig. 5K,L). High-speed video microscopy of 30-hpf control embryos and *sept7b* morphants revealed that the beat frequency of the distal pronephric cilia was significantly slower in *sept7b* morphants (21.17±2.71 Hz, $n=10$ compared with 27.76±1.35 in the controls, mean±s.d., $n=6$; $P<0.05$), and that the pattern of beating was also irregular in the morphants (supplementary material Fig. S4; Movies 1 and 2). Note that our analysis could have missed some short cilia. Taken together, these data indicate that knockdown of *sept7b* leads to misorientation of basal bodies and cilia, and a concomitant lack of directional fluid flow in the pronephros.

Depletion of *sept7b* reduces apical actin in pronephric tubules

Septins associate with actin (Kinoshita et al., 2002; Kinoshita et al., 1997), and knockdown of septins has been shown to disassemble or destabilize actin bundles in cultured cells (Kinoshita et al., 2002); thus, we tested whether knockdown of *sept7b* in zebrafish led to abnormal organization of actin. Indeed, the staining with phalloidin of 3.5-dpf larvae that had been injected with the TBMO-MM control or the *sept7b* TBMO revealed a reduced accumulation of actin on the apical surface of pronephric tubule cells in *sept7b* morphants compared with the control ($n=13$ for each) (Fig. 6).

Knockdown of *sept7b* causes defects in left–right asymmetry and hydrocephaly

We next examined whether knockdown of *sept7b* levels affected left–right asymmetry, which is sensitive to defects in cilia function. *In situ* hybridization for *southpaw* (*spaw*), an early marker of left–right asymmetry (Long et al., 2003), showed that *spaw* was expressed in the left-side lateral plate mesoderm in most of the control embryos (276 of 314; Fig. 7A,G). In *sept7b* morphants, *spaw* expression was more random and was detected in either the right-side lateral plate mesoderm (69 of 299), bilaterally (75 of 299) or was absent (36 of 299) (Fig. 7B,C,G). We also examined the expression of *cmlc2*, a marker for the heart (Yelon et al., 1999), and found that in the majority of control embryos (200 of 203) the heart tube was shifted to the left (Fig. 7D,H); by contrast, in *sept7b*-TBMO-injected embryos, *cmlc2* expression was more random (to the left in 130 of 219 embryos; in the center or to the right in 89 of 219 embryos) (Fig. 7E,F,H). We also observed that *sept7b* morphants displayed hydrocephaly (Fig. 7I–L), supporting the hypothesis that there is a function for *sept7b* in the regulation of ciliogenesis and fluid flow. Analysis by confocal microscopy further confirmed that the ependymal cilia of the central canal, which were stained for acetylated tubulin, appeared short, misoriented and reduced in number in *sept7b*-TBMO-injected zebrafish compared with the controls (Fig. 7M,N).

Septin 7 physically interacts with Rab8

The distribution of septin 7 in the cytoplasm of ciliated cells in zebrafish suggests that septin 7 could have roles that are additional to its function as a ciliary membrane diffusion barrier (Chih et al., 2011; Hu et al., 2010) or a possible component of the ciliary axoneme (Ghossoub et al., 2013). As septins are known to function in vesicle trafficking (Beites et al., 1999; Hsu et al., 1998; Wasik et al., 2012), we hypothesized that septin 7 could be involved in the trafficking processes associated with ciliogenesis. The small GTPase Rab8 functions in vesicle trafficking and is a central regulator of cilium formation (Nachury et al., 2007; Yoshimura et al., 2007). We found that Rab8 and septin 7 partially colocalized in a punctate vesicule-like pattern in mIMCD3 cells (Fig. 8A–C). Furthermore, two different antibodies directed against septin 7 co-immunoprecipitated Rab8, indicating that septin 7 and Rab8 physically interact (Fig. 8D). These data suggest that septin 7 might function together with Rab8 in vesicle trafficking that is involved in ciliogenesis.

DISCUSSION

We showed that *sept7b* is essential for both the glomerular and tubular function of the pronephric kidney in zebrafish. Septin 7 localized to ciliated cells of the pronephric tubules and to the ciliated cells of other tissues. Notably, knockdown of *sept7b* resulted in disruption of motile and non-motile ciliogenesis. This led to defects in fluid flow and, thereby, to the formation of pronephric cysts and edema, hydrocephaly and to abnormalities in left–right asymmetry. A number of genes are involved in regulating ciliogenesis and cilia function – including genes that control basal body formation and localization, intraflagellar transport, integrity of the axoneme and cytoskeletal organization (Cao et al., 2010; Essner et al., 2005; Kramer-Zucker et al., 2005a; Ravanelli and Klingensmith, 2011; Sullivan-Brown et al., 2008; Sun et al., 2004). Our study links the role of septins in ciliogenesis (Hu et al., 2010; Kim et al., 2010) to the function of several vertebrate tissues – including the kidney, central canal and Kupffer's vesicle – that require cilia *in vivo*.

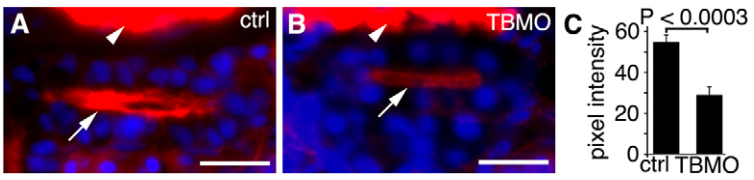

Fig. 6. Apical actin is reduced in the pronephric tubule epithelia of *sept7b*-knockdown larvae. (A,B) Staining with phalloidin shows prominent apical actin (arrows) in the pronephric tubule of larvae injected with the TBMO-MM control (ctrl; A). By contrast, the intensity of actin staining is reduced in larvae injected with the *sept7b* TBMO (TBMO, B). The arrowheads point to muscle with intense labeling for actin. DAPI (blue) stains the nuclei. (C) The fluorescence intensity of actin staining in the pronephric tubules is reduced in *sept7b* morphants. The same settings were used during imaging of control and morphant larvae, and the images were analyzed without processing. Scale bars: 10 μm.

Journal of Cell Science

Journal of Cell Science (2014) 127, 1476–1486 doi:10.1242/jcs.138495

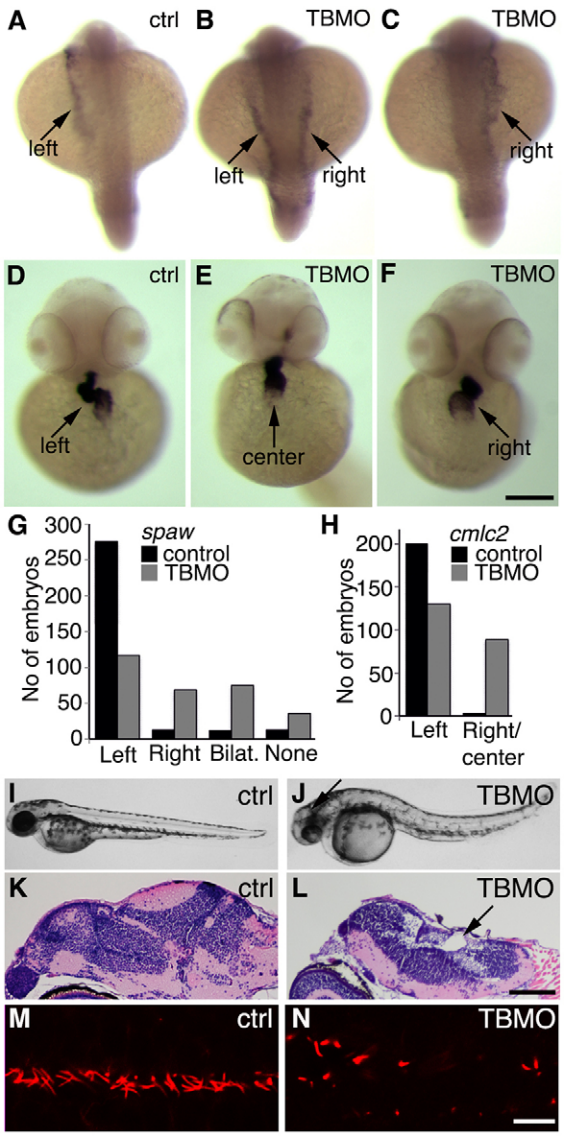

Fig. 7. Suppression of *sept7b* leads to defects in left–right asymmetry and hydrocephaly. (A–C) *In situ* hybridization of *spaw* in control (ctrl) embryos at the 20-somite stage (A) and in embryos treated with the *sept7b* TBMO (B,C). *Spaw* is expressed in the left lateral plate mesoderm in control embryos (A), whereas *spaw* expression is bilateral (B) or in the right lateral plate (C) in *sept7b* morphants, as indicated by arrows. (D–F) *In situ* hybridization of *cmlc2* in a control embryo at the 30-somite stage (D) and in *sept7b* TBMO morphants (E,F). *Cmlc2* expression shows the heart tube looping to the left in control embryos (D), whereas *cmlc2* expression is in the center (E) or looping to the right (F) in *sept7b* morphants, as indicated by arrows. (G) The number of control and *sept7b* morphant embryos with *spaw* expression on the left side, right side, bilaterally or absent. (H) The number of control and *sept7b*-morphant embryos with *cmcl2* expression on the left side, in the center or on the right side. (I,J) 2-dpf control embryos (I). (J) *sept7b* morphant (TBMO) at 2 dpf shows hydrocephaly (arrow). (K,L) Histological sections stained with hematoxylin–eosin of 4-dpf control (K) and TBMO-injected (L) zebrafish larvae show hydrocephalus in the morphants (arrow). (M,N) Immunofluorescence staining for acetylated tubulin (red) reveals misorientation, shortening and a reduced number of cilia in 30-hpf zebrafish that had been injected with the TBMO (N) compared with the control (M). Scale bars: 130 μm (A–F); 100 μm (K,L); 10 μm (M,N).

sept7b is widely expressed at the early stages of zebrafish development. The presence of the transcript in fertilized embryos indicates the maternal accumulation of *sept7b* mRNA in zebrafish embryos (Kimmel et al., 1995). In zebrafish embryos, we found that septin 7 is expressed in tissues with cells that have motile or primary cilia, including the pronephric kidney. Similarly, septin 7 is prominently expressed in the rat in kidney glomerular epithelial and tubular cells (Wasik et al., 2012), the brain and lung, and at a lower level in the pancreas and testis (Hsu et al., 1998). In the ciliated cells in the zebrafish, septin 7 is localized to the epithelium, at the base of the cilium and along the ciliary axoneme, depending on the tissue analyzed. This kind of wide expression and variation of localization that is dependent on the cell type corresponds to the previously published localization of septin 7 in cultured cells and *Xenopus* embryos (Ghossoub et al., 2013; Kim et al., 2010). In cultured retinal pigmented epithelial cells, septin 7 localizes to the cytoplasm and a small proportion of the protein is found along extended mature primary cilia (Ghossoub et al., 2013). In the multi-ciliated cells of *Xenopus* epidermis, septin 7 is found at the base of the cilia and along the ciliary axoneme (Kim et al., 2010). Differences in the localization of septin 7 in a variety of cell types might reflect different functions for septin 7 in the regulation of ciliogenesis or mature cilia, such as the formation of a diffusion barrier at the base of the cilia (Chih et al., 2011; Hu et al., 2010), or as a component of the ciliary axoneme (Ghossoub et al., 2013).

Knockdown of *sept7b* by using two different morpholino antisense oligonucleotides gave similar phenotypes. A mismatched morpholino antisense oligonucleotide did not cause any phenotypic differences, and *sept7b* mRNA rescued the *sept7b* morphant phenotypes. There are two paralogous septin 7 genes in zebrafish, *sept7a* and *sept7b*. Because knockdown of *sept7b* resulted in specific developmental defects, it is unlikely that *sept7a* functionally compensates for *sept7b*.

Light microscopy analysis of *sept7b* morphants revealed an expansion of the Bowman's space – resembling that observed in *pkd2* morphants and *locke* (*to237b*) mutants (Obara et al., 2006; Sullivan-Brown et al., 2008; Zhao and Malicki, 2007) – and electron microscopy analysis showed changes in the podocytes of *sept7b* morphants that were similar to those in *nephrin* and *mosaic eyes* morphants (Kramer-Zucker et al., 2005b). We further showed that *sept7b* is essential for maintaining the functional integrity of the glomerular filtration barrier. This is in line with our previous finding that septin 7 also interacts with proteins essential for maintaining podocyte structure and glomerular filtration function (Wasik et al., 2012).

Staining for acetylated tubulin revealed a significant reduction in the length of cilia in the dilated pronephric tubules in *sept7b* morphants and this resembled several other mutants and morphants that lead to defective pronephric function (Clément et al., 2011; Kramer-Zucker et al., 2005a; Ravanelli and Klingensmith, 2011; Sun et al., 2004). The cilia and basal bodies of the *sept7b* morphants were also misoriented and resembled the phenotype of zebrafish with mutations in intraflagellar transport proteins that cause defects in basal body orientation and planar polarity (Cao et al., 2010; Jones et al., 2008). Components of the planar cell polarity (PCP) pathway have also been shown to regulate the apical docking and planar polarization of basal bodies (Park et al., 2008). In *Xenopus* embryos, septin 7 functions together with the PCP protein Fritz (*wdpcp*) to regulate both collective cell movement and ciliogenesis (Kim et al., 2010). It is possible that lack of *sept7b*

Journal of Cell Science (2014) 127, 1476–1486 doi:10.1242/jcs.138495

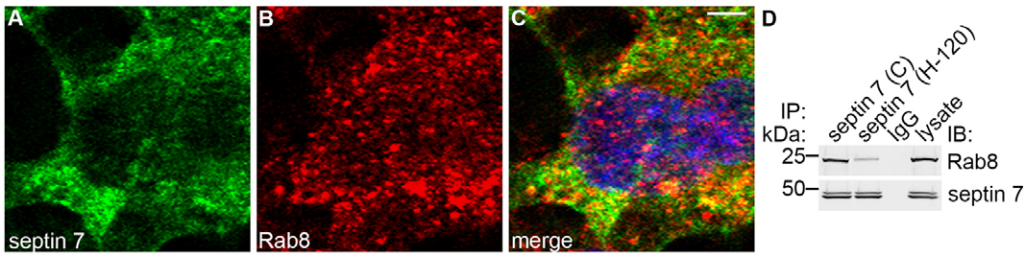

Fig. 8. Septin 7 forms a complex with Rab8. (A–C) Immunofluorescence staining of mIMCD3 cells shows partial colocalization of septin 7 (A) and Rab8 (B) in the perinuclear region, as shown by the yellow coloring in the merged image (C). Scale bar: 10 μm. (D) Two different septin 7 antibodies (C or H-120) co-immunoprecipitate Rab8 in mIMCD3 cell lysates, indicating that septin 7 and Rab8 physically interact. IP, immunoprecipitation; IB, immunoblotting.

in zebrafish affects the function of the PCP pathway and, thereby, basal body polarity and ciliogenesis. Alternatively, reduction of the motility of the cilia and, thereby, reduction of fluid flow, as observed in *sept7b* knockdown zebrafish here, can also lead to randomized organization of cilia (Mitchell et al., 2007). Furthermore, the PCP protein Vangl2 links external hydrodynamic forces to intracellular PCP signaling and the position and orientation of cilia (Borovina et al., 2010; Guirao et al., 2010). Taken together, these data indicate that the PCP pathway and fluid flow act together to orient cilia, and either pathway, or both, could be involved in the manifestation of the ciliogenesis defect that follows *sept7b* knockdown.

Interestingly, we found that apical actin levels appeared to be reduced in the pronephric tubular cells after *sept7b* depletion. Because a well-organized actin cytoskeleton is required for the migration and docking of the basal bodies to the apical plasma membrane, and for cilia elongation (Boisvieux-Ulrich et al., 1990; Pan et al., 2007; Ravanelli and Klingensmith, 2011; Tamm and Tamm, 1988), a *sept7b*-dependent disruption of actin organization could contribute to the defects in ciliogenesis. Alternatively, the reduced number of basal bodies upon *sept7b* knockdown could also lead to reduced cortical actin, as a dense apical actin cap has been shown to form around basal bodies after their apical docking (Pan et al., 2007; Werner et al., 2011). In addition, a sub-apical actin network connects neighboring cilia to coordinate the synchronized beating of cilia (Werner et al., 2011). Reduced apical actin could also explain the paucity and irregular shapes of microvilli that have been observed in the epithelia in *sept7b* morphants (Boisvieux-Ulrich et al., 1990). Interestingly, and similar to *sept7b*, the PCP effectors *inturned* and *fuzzy* have been shown to participate in the assembly of apical actin filaments. Additionally, similar to upon knockdown of *sept7b*, depletion of *inturned* or *fuzzy* leads to defects in ciliogenesis (Park et al., 2006). Collectively, *sept7b* expression is required for ciliogenesis in epithelial cells that line the pronephric tubule and, consequently, for fluid flow and the proper function of the pronephros.

Other typical signs of ciliary dysfunction observed in our study included defects in left–right asymmetry and hydrocephaly. Development of left–right asymmetry in zebrafish depends on cilia-induced directional fluid flow in Kupffer's vesicle, which leads to the asymmetric expression of genes, and defects in cilia structure or function cause randomization of organ patterning (Essner et al., 2005). In *sept7b* morphants, the normal asymmetry of two different markers, *spaw* (lateral plate mesoderm) and *cmlc2* (a heart marker), was randomized. Similar defects in asymmetrical organ patterning, kidney function and ciliogenesis have been observed in *cdc14B* phosphatase morphants and mutants, and actin nucleator *cordon-bleu* morphants (Clément et al., 2011; Ravanelli and Klingensmith, 2011).

We found that in mIMCD3 cells septin 7 physically interacts with Rab8, a small GTPase that functions in ciliogenesis by targeting vesicles to the cilium and promoting elongation of the ciliary membrane (Nachury et al., 2007; Yoshimura et al., 2007). Interestingly, Rab8 is involved in the development of Kupffer's vesicle in zebrafish (Nachury et al., 2007) and regulates vesicle trafficking in *Xenopus* photoreceptors (Moritz et al., 2001). Furthermore, knockdown of Rab8 in *cc2d2a* mutant zebrafish enhances pronephric cyst formation (Bachmann-Gagescu et al., 2011). Further studies are required to define whether Rab8 and septin 7 function together in the regulation of vesicle trafficking and, thereby, ciliogenesis in these tissues.

In summary, our work identifies a physiological role for septin 7 in the maintenance of the functionality of several tissues *in vivo* that is dependent on functional cilia. Septin 7 might affect ciliogenesis and ciliary function as a component of the PCP pathway, or by regulating actin cytoskeleton organization or vesicle trafficking. Our results elucidate a role of septins that underlies the defective functions of motile or primary cilia that are associated with a number of human diseases (ciliopathies) (Bisgrove and Yost, 2006; Eley et al., 2005; Hildebrandt et al., 2011). A large number of genes are responsible for these ciliopathies, and the expression pattern of those genes and their roles in regulating the ciliary function vary in different cell and tissue types that lead to diverse phenotypes (Bisgrove and Yost, 2006). In zebrafish, septin 7 is expressed in cells with motile or primary cilia, and the phenotype of *sept7b* morphants resembles that of several human ciliopathies. *sept7b* is also required for the integrity of the glomerular filtration apparatus. It will be of interest to analyze whether septin 7 mutations or mis-expression are also associated with renal disease in humans.

MATERIALS AND METHODS

Zebrafish lines

The wild-type Turku zebrafish line and *wt1b::GFP* transgenic line (a kind gift from Christoph Englert, Leibniz Institute for Age Research, Fritz Lipmann Institute, Germany) were maintained and raised as described previously (Westerfield, 2000). The *wt1b::GFP* transgenic line expresses GFP under the control of the *wt1b* promotor; thereby, GFP expression is localized specifically in pronephric regions (Perner et al., 2007). Embryos were staged according to somite number or hours or days post fertilization (Kimmel et al., 1995).

Cloning of *sept7b*

The zebrafish *sept7b* sequence (NCBI Reference Sequence: NM_001077743.1, zgc: 153214) was identified by tblastn search using

the zebrafish genome assembly (Sanger Institute, UK, http://www.ensembl.org/Danio_rerio/). Total RNA was isolated from 30 embryos (72 hpf) using the RNeasy mini Kit (Qiagen, Hilden, Germany) and reverse-transcribed with random hexamer primers and Superscript III reverse transcriptase (Invitrogen, Carlsbad, CA) following manufacturers' protocols. The full-length coding sequence of zebrafish *sept7b* was amplified using primers *sept7b*-1F and *sept7b*-1R (supplementary material Table S1), and subcloned into the pGEM-T Easy vector (Promega, Madison, WI). The quality of the cDNA was confirmed by zebrafish *rps3* (ribosomal protein subunit 3, NCBI Reference Sequence: NM_201153.1; zgc: 56088) using primers *rps3*-1F and *rps3*-1R (supplementary material Table S1).

Whole-mount *in situ* hybridization

The *sept7b* probe sequence was amplified from cDNA that had been prepared as described above using the primers *sept7b*-2F and *sept7b*-2R (supplementary material Table S1) and then subcloned into the pGEM-T Easy vector. Insertion of the sequence into the vector was confirmed by sequencing. Southpaw (*spaw*) and cardiac myosin light chain 2 (*cmlc2*) constructs were a kind gift from Didier Stainier (University of California San Francisco, San Francisco, CA). The probes were labeled using the Digoxigenin labeling kit (Roche, Mannheim, Germany). Whole-mount *in situ* hybridization was performed as described previously (Thisse and Thisse, 2008), using an antibody against digoxigenin that had been conjugated with alkaline phosphatase and nitro-blue tetrazolium with 5-bromo-4-chloro-3′-indolyphosphate (Roche) for detection. If embryos were used for analyses after 24 hpf, they were transferred to E3 medium containing 0.003% 1-phenyl 2-thiourea to prevent pigmentation. Embryos were fixed in 4% paraformaldehyde (PFA) at 4℃ overnight at the 20-somite stage for *spaw*, 30 hpf for *cmlc2* and 3 hpf or 4 dpf for *sept7b*.

Immunohistochemistry

For whole-mount immunostaining, zebrafish larvae at 3 or 4 dpf were fixed in 4% PFA at 4℃ overnight followed by Dent's fixative (80% methanol, 20% DMSO; Kramer-Zucker et al., 2005a) at −20℃ for 3–4 h. Samples were blocked with 15% normal goat serum (Sigma-Aldrich, St Louis, MO) in blocking solution (PBDT; PBS containing 1% BSA, 1% DMSO, 0.5% Tween-20, 0.1% Triton X-100) and incubated with a rabbit polyclonal antibody against septin 7 (C, Immuno-Biological Laboratories, Gumma, Japan or H-120, Santa Cruz Biotechnology, Dallas, TX) in blocking solution at 4℃ overnight followed by detection with Alexa-Fluor-488-conjugated donkey anti-rabbit IgG (Invitrogen).

For the detection of cilia or basal bodies, embryos were fixed in Dent's fixative at 4℃ overnight, blocked as above, and incubated with a monoclonal antibody against acetylated α-tubulin 6-11B-1, a rabbit polyclonal antibody against γ-tubulin (Sigma-Aldrich) and/or a rabbit polyclonal antibody against septin 7, followed by detection with Alexa-Fluor-568-conjugated goat anti-mouse and Alexa-Fluor-488-conjugated goat anti-rabbit IgGs (Invitrogen). Samples were mounted in Vectashield (Vector Laboratories, Burlingame, CA) and images were acquired by using a Leica SP2 or Leica SP8 confocal microscope with extended focus (Leica Microsystems CMS GmbH, Mannheim, Germany). The confocal *z*-stack images were reconstructed by Imaris 7.5 software (BITPLANE Scientific Software, Zurich, Switzerland). The length of pronephric cilia was measured from 21 embryos per group, 10–12 cilia per embryo, and Kupffer's vesicle cilia from 16 embryos per group, 20–25 cilia per embryo, using Image J 1.43u as described previously (Jaffe et al., 2010).

For immunohistochemistry, zebrafish larvae at 4 dpf were fixed in 4% PFA at 4℃ overnight, incubated in 30% sucrose solution at 4℃ overnight and embedded in Tissue Tek (Sakura Finetek Europe B.V., Alphen aan den Rijn, Netherlands). Sections of 8 µm were fixed in acetone at −20℃ for 10 min and then blocked with C-Block (Genemed Biotechnologies, South San Francisco, CA). The sections were incubated with rhodamine–phalloidin (Molecular Probes, Life Technologies, Carlsbad, CA) or a rabbit polyclonal antibody against septin 7 diluted in Dako REAL Antibody Diluent (Dako, Glostrup, Denmark) at 4℃ overnight, followed by detection with Alexa-Fluor-555-conjugated donkey anti-rabbit IgG. Samples were mounted and imaged as described above. For measuring the fluorescence intensity of actin, samples were imaged by using a Zeiss Axioplan2 microscope (Carl Zeiss Microscopy GmbH, Jena, Germany). Constant settings were maintained and a fixed area covering the tubular region of each sample was quantified using Image J 1.43u software.

mIMCD3 cells were cultured in Dulbecco's modified Eagle's medium (DMEM)-F12 supplemented with 10% fetal bovine serum, 1% glutamax and 1% penicillin-streptomycin. Cells were fixed with PFA, permeabilized with Triton X-100 and then stained with a mouse antibody against Rab8 (BD Transduction Laboratories™, San Jose, CA) and a rabbit antibody against septin 7 (C) followed by detection with Alexa-Fluor-555-conjugated donkey anti-mouse and Alexa-Fluor-488-conjugated donkey anti-rabbit IgGs. Imaging was performed by using a Leica SP8 confocal microscope.

Morpholino antisense oligonucleotide injections

The morpholino antisense oligonucleotides *sept7b* TBMO, *sept7b* SBMO-2, control TBMO-MM and p53 (Robu et al., 2007) (supplementary material Table S1) were obtained from Gene Tools (LLC, Philomath, OR) and 6–8 ng of TBMO and 10–12 ng of SBMO-2 was injected into fertilized eggs using a PLI-90 microinjector (Harvard Apparatus, Cambridge, MA). The effect of the splice-blocking *sept7b* morpholino antisense oligonucleotide was verified by PCR using the primers *sept7b*-3F and *sept7b*-3R, and by qRT-PCR using the primers *sept7b*-4F and *sept7b*-4R (supplementary material Table S1). The values were normalized using *rps3* that had been amplified using the primers *rps3*-2F and *rps3*-2R (supplementary material Table S1). qRT-PCR was performed using the Power SYBR Green PCR Master Mix (Applied Biosystems, Carlsbad, CA) in an iCycler iQTM Real-Time PCR Detection System (Bio-Rad Laborotories, Hercules, CA).

Rescue experiments

250 pg of full-length zebrafish *sept7b* capped mRNA, which had been synthesized by *in vitro* transcription by using the mMESSAGE mMACHINE T7 RNA synthesis kit (Ambion by Life Technologies, Carlsbad, CA), was co-injected into embryos with the morpholino antisense oligonucleotides. The expression level of *sept7b* mRNA in rescued embryos was analyzed by using qRT-PCR using the zebrafish *sept7b* primers *sept7b*-5F and *sept7b*-5R. The expression levels were normalized against *rps3* that had been amplified by using the primers *rps3*-2F and *rps3*-2R (supplementary material Table S1).

Western blotting

At 2 and 4 dpf, control zebrafish larvae or those that had been injected with morpholino antisense oligonucleotides were lysed in RIPA buffer [150 mM NaCl, 1% Nonidet P-40 (NP-40), 0.5% sodium deoxycholate, 0.1% sodium dodecyl sulfate (SDS) and 50 mM Tris-HCl pH 8.0] supplemented with 50 mM NaF, 1× protease inhibitor cocktail (EDTA-free, Roche, Germany) and 1 mM Na_3VO_4 using a 20-gauge needle. Insoluble material was removed by centrifugation at 10,000 ***g*** at 4℃ for 10 min. Lysates were denatured in Laemmli buffer, and proteins were separated by SDS-PAGE. Western blotting was performed by using a rabbit polyclonal antibody against septin 7 (Santa Cruz Biotechnology, Santa Cruz, CA) and a monoclonal mouse antibody against actin (Sigma-Aldrich) followed by Alexa-Fluor-680-conjugated donkey anti-rabbit (Invitrogen) and IR-Dye-800-conjugated donkey anti-mouse IgGs (LI-COR, Lincoln, NE).

Histology and electron microscopy

In situ hybridized 4-dpf control and larvae that had been injected with morpholino antisense oligonucleotides were post-fixed in 2% glutaraldehyde in 0.1 M phosphate buffer at room temperature overnight, dehydrated in ethanol and embedded in LX112 (Ladd Research, Williston, VT). Semi-thin (0.2-µm) transverse sections were stained with toluidine blue and photographed by using a Nikon Eclipse 800 microscope equipped with Spot Image digital camera. For electron microscopy, larvae at 4 dpf were fixed in 1.6% paraformaldehyde and 2.5% glutaraldehyde in 0.1 M phosphate buffer, pH 7.2, at room temperature for 4 h, postfixed in 1% osmium tetraoxide at room

Journal of Cell Science

temperature for 1 h, dehydrated in ethanol and embedded in LX112. Thin sections (100-nm) were stained with uranyl acetate and lead citrate and examined in a JEOL 1400 electron microscope that was equipped with an Olympus-SIS Morada digital camera. The angle between cilia was measured by using the images as previously described (De Iongh and Rutland, 1989) and the ITEM software that was provided with the JEOL 1400 electron microscope.

Dextran uptake and renal clearance assays

Fluorescein dextrans (10,000- or 500,000-kDa, Invitrogen; 1 mg/ml) were injected into the pericardinal vein of transiently anesthetized [0.003% Tricaine (MS-222); Sigma-Aldrich] zebrafish larvae at 3.5 dpf. The larvae were fixed with 4% PFA 1.5 h after injection, embedded in OCT compound and sectioned, and the endocytosis of fluorescein dextrans into the pronephric tubule was examined by using a Zeiss Axioplan2 microscope (Carl Zeiss Microscopy GmbH, Jena, Germany) (Kramer-Zucker et al., 2005b; Mitra et al., 2012). For the renal clearance assay, tetramethylrhodamine dextran (70,000-kDa; Invitrogen) was injected into the pericardial sac of transiently anesthetized 53-hpf zebrafish embryos, as described previously (Mitra et al., 2012; Rothschild et al., 2011). Embryos were imaged within 20 min of injection and again at 77 hpf. Reduction of rhodamine–dextran from the pericardial sac and anterior embryo was examined by using a Zeiss Axiovert 200 inverted microscope and recorded by using the Zeiss AxioVision 3.1 software. The heartbeat of the dye-injected control and *sept7b*-morphant larvae was measured as previously described (Mitra et al., 2012) and reported as beats per minute.

High-speed video microscopy

Phenylthiourea-treated 30-hpf zebrafish embryos were transiently anesthetized with 0.003% tricaine and imaging of cilia beating was conducted by using an inverted IX70 microscope (Olympus Corporation, Germany) equipped with a UAPo ×40/1.15 water objective (Olympus). Images were recorded by using a Hamamatsu ORCA-Flash 4.0 sCMOS camera (Hamamatsu Photonics K.K., Japan) at 250 frames per second. Data acquisition was controlled and the recordings were analyzed by using HCImage software (Hamamatsu Photonics K.K., Japan). The images were processed by using Image J software. The beating rates of cilia were counted and averaged from three 1-s intervals. Additionally, the beating rate was quantified by measuring changes in light intensity over a region of interest that had been selected next to each cilium.

Immunoprecipitation

mIMCD3 cells were lysed in NP-40 buffer (1% NP-40, 20 mM Hepes, pH 7.5, 150 mM NaCl) supplemented with 50 mM NaF, 1 mM Na_3VO_4 and 1× complete protease inhibitor cocktail (Roche, Basel, Switzerland) as described previously (Wasik et al., 2012). Lysates were pre-cleared with TrueBlot® anti-rabbit Ig immunoprecipitation beads (eBiosciences, San Diego, CA) and incubated with antibodies against septin 7 (C or H120) or rabbit IgG (Zymed, South San Francisco, CA) at 4℃ for 16 h. The immune complexes were bound to TrueBlot beads, washed with lysis buffer and immunoblotted with a mouse antibody against Rab8 and a rabbit antibody against septin 7 (C).

Statistics

The significance of differences was analyzed by using a two-tailed Student's *t*-test. Error bars on the graphs show the standard deviation.

Acknowledgements

The transgenic *wt1b::GFP* zebrafish line was kindly provided by Christoph Englert (Leibniz Institute for Age Research, Fritz Lipmann Institute, Germany), and the *spaw* and *cmlc2* constructs by Didier Stainier (UCSF, San Francisco, CA). We thank Emmi Kasurinen, Jussi Kenkkilä, Antti Isomäki, Ulla Kiiski, Henri Koivula, Mikko Liljestörm, Susanna Norrback, Niina Ruoho, Fang Zhao and Svetlana Zueva for their help and technical support.

Competing interests

The authors declare no competing interests.

Author contributions

S.N.D., E.L., A.A.W., A.S. and J.P. performed and analyzed the experiments. P.P. provided expertise on working with zebrafish. S.N.D., A.S., W.J.N. and S.L. designed the experiments. S.N.D., W.J.N. and S.L. wrote the manuscript. All co-authors corrected the manuscript.

Funding

This work was supported by the European Research Council [grant number 242820 to S.L.); the Academy of Finland [grant numbers 121248, 131255 and 218021 to S.L.]; the Helsinki Biomedical Graduate Program (to A.A.W.); the National Institutes of Health [grant number GM35527 to W.J.N.]; a Marie Curie International Outgoing Fellowship (A.S.); J.P. was supported by the Finnish Medical Foundation/The Finnish Medical Society Duodecim. Deposited in PMC for release after 12 months.

Supplementary material

Supplementary material available online at
http://jcs.biologists.org/lookup/suppl/doi:10.1242/jcs.138495/-/DC1

References

Bachmann-Gagescu, R., Phelps, I. G., Stearns, G., Link, B. A., Brockerhoff, S. E., Moens, C. B. and Doherty, D. (2011). The ciliopathy gene *cc2d2a* controls zebrafish photoreceptor outer segment development through a role in Rab8-dependent vesicle trafficking. *Hum. Mol. Genet.* **20**, 4041-4055.

Beites, C. L., Xie, H., Bowser, R. and Trimble, W. S. (1999). The septin CDCrel-1 binds syntaxin and inhibits exocytosis. *Nat. Neurosci.* **2**, 434-439.

Bisgrove, B. W. and Yost, H. J. (2006). The roles of cilia in developmental disorders and disease. *Development* **133**, 4131-4143.

Boisvieux-Ulrich, E., Lainé, M.-C. and Sandoz, D. (1990). Cytochalasin D inhibits basal body migration and ciliary elongation in quail oviduct epithelium. *Cell Tissue Res.* **259**, 443-454.

Borovina, A., Superina, S., Voskas, D. and Ciruna, B. (2010). Vangl2 directs the posterior tilting and asymmetric localization of motile primary cilia. *Nat. Cell Biol.* **12**, 407-412.

Bowen, J. R., Hwang, D., Bai, X., Roy, D. and Spiliotis, E. T. (2011). Septin GTPases spatially guide microtubule organization and plus end dynamics in polarizing epithelia. *J. Cell Biol.* **194**, 187-197.

Cao, Y., Park, A. and Sun, Z. (2010). Intraflagellar transport proteins are essential for cilia formation and for planar cell polarity. *J. Am. Soc. Nephrol.* **21**, 1326-1333.

Chih, B., Liu, P., Chinn, Y., Chalouni, C., Komuves, L. G., Hass, P. E., Sandoval, W. and Peterson, A. S. (2011). A ciliopathy complex at the transition zone protects the cilia as a privileged membrane domain. *Nat. Cell Biol.* **14**, 61-72.

Clément, A., Solnica-Krezel, L. and Gould, K. L. (2011). The Cdc14B phosphatase contributes to ciliogenesis in zebrafish. *Development* **138**, 291-302.

De Iongh, R. and Rutland, J. (1989). Orientation of respiratory tract cilia in patients with primary ciliary dyskinesia, bronchiectasis, and in normal subjects. *J. Clin. Pathol.* **42**, 613-619.

Drummond, I. A., Majumdar, A., Hentschel, H., Elger, M., Solnica-Krezel, L., Schier, A. F., Neuhauss, S. C. F., Stemple, D. L., Zwartkruis, F., Rangini, Z. et al. (1998). Early development of the zebrafish pronephros and analysis of mutations affecting pronephric function. *Development* **125**, 4655-4667.

Ebarasi, L., Oddsson, A., Hultenby, K., Betsholtz, C. and Tryggvason, K. (2011). Zebrafish: a model system for the study of vertebrate renal development, function, and pathophysiology. *Curr. Opin. Nephrol. Hypertens.* **20**, 416-424.

Eley, L., Yates, L. M. and Goodship, J. A. (2005). Cilia and disease. *Curr. Opin. Genet. Dev.* **15**, 308-314.

Essner, J. J., Amack, J. D., Nyholm, M. K., Harris, E. B. and Yost, H. J. (2005). Kupffer's vesicle is a ciliated organ of asymmetry in the zebrafish embryo that initiates left-right development of the brain, heart and gut. *Development* **132**, 1247-1260.

Ghossoub, R., Hu, Q., Failler, M., Rouyez, M.-C., Spitzbarth, B., Mostowy, S., Wolfrum, U., Saunier, S., Cossart, P., Jamesnelson, W. et al. (2013). Septins 2, 7 and 9 and MAP4 colocalize along the axoneme in the primary cilium and control ciliary length. *J. Cell Sci.* **126**, 2583-2594.

Guirao, B., Meunier, A., Mortaud, S., Aguilar, A., Corsi, J.-M., Strehl, L., Hirota, Y., Desoeuvre, A., Boutin, C., Han, Y.-G. et al. (2010). Coupling between hydrodynamic forces and planar cell polarity orients mammalian motile cilia. *Nat. Cell Biol.* **12**, 341-350.

Hall, P. A., Jung, K., Hillan, K. J. and Russell, S. E. H. (2005). Expression profiling the human septin gene family. *J. Pathol.* **206**, 269-278.

Hartwell, L. H. (1971). Genetic control of the cell division cycle in yeast. IV. Genes controlling bud emergence and cytokinesis. *Exp. Cell Res.* **69**, 265-276.

Hildebrandt, F., Benzing, T. and Katsanis, N. (2011). Ciliopathies. *N. Engl. J. Med.* **364**, 1533-1543.

Hsu, S.-C., Hazuka, C. D., Roth, R., Foletti, D. L., Heuser, J. and Scheller, R. H. (1998). Subunit composition, protein interactions, and structures of the mammalian brain sec6/8 complex and septin filaments. *Neuron* **20**, 1111-1122.

Hu, Q., Milenkovic, L., Jin, H., Scott, M. P., Nachury, M. V., Spiliotis, E. T. and Nelson, W. J. (2010). A septin diffusion barrier at the base of the primary cilium maintains ciliary membrane protein distribution. *Science* **329**, 436-439.

Hu, J., Bai, X., Bowen, J. R., Dolat, L., Korobova, F., Yu, W., Baas, P. W., Svitkina, T., Gallo, G. and Spiliotis, E. T. (2012). Septin-driven coordination of actin and microtubule remodeling regulates the collateral branching of axons. *Curr. Biol.* **22**, 1109-1115.

Jaffe, K. M., Thiberge, S. Y., Bisher, M. E. and Burdine, R. D. (2010). Imaging cilia in zebrafish. *Methods Cell Biol.* **97**, 415-435.

Joberty, G., Perlungher, R. R., Sheffield, P. J., Kinoshita, M., Noda, M., Haystead, T. and Macara, I. G. (2001). Borg proteins control septin organization and are negatively regulated by Cdc42. *Nat. Cell Biol.* **3**, 861-866.

Jones, C., Roper, V. C., Foucher, I., Qian, D., Banizs, B., Petit, C., Yoder, B. K. and Chen, P. (2008). Ciliary proteins link basal body polarization to planar cell polarity regulation. *Nat. Genet.* **40**, 69-77.

Jorissen, M. and Willems, T. (2004). The secondary nature of ciliary (dis)orientation in secondary and primary ciliary dyskinesia. *Acta Otolaryngol.* **124**, 527-531.

Kestilä, M., Lenkkeri, U., Männikkö, M., Lamerdin, J., McCready, P., Putaala, H., Ruotsalainen, V., Morita, T., Nissinen, M., Herva, R. et al. (1998). Positionally cloned gene for a novel glomerular protein—nephrin—is mutated in congenital nephrotic syndrome. *Mol. Cell* **1**, 575-582.

Kim, C. S., Seol, S. K., Song, O.-K., Park, J. H. and Jang, S. K. (2007). An RNA-binding protein, hnRNP A1, and a scaffold protein, septin 6, facilitate hepatitis C virus replication. *J. Virol.* **81**, 3852-3865.

Kim, S. K., Shindo, A., Park, T. J., Oh, E. C., Ghosh, S., Gray, R. S., Lewis, R. A., Johnson, C. A., Attie-Bittach, T., Katsanis, N. et al. (2010). Planar cell polarity acts through septins to control collective cell movement and ciliogenesis. *Science* **329**, 1337-1340.

Kimmel, C. B., Ballard, W. W., Kimmel, S. R., Ullmann, B. and Schilling, T. F. (1995). Stages of embryonic development of the zebrafish. *Dev. Dyn.* **203**, 253-310.

Kinoshita, M., Kumar, S., Mizoguchi, A., Ide, C., Kinoshita, A., Haraguchi, T., Hiraoka, Y. and Noda, M. (1997). Nedd5, a mammalian septin, is a novel cytoskeletal component interacting with actin-based structures. *Genes Dev.* **11**, 1535-1547.

Kinoshita, A., Kinoshita, M., Akiyama, H., Tomimoto, H., Akiguchi, I., Kumar, S., Noda, M. and Kimura, J. (1998). Identification of septins in neurofibrillary tangles in Alzheimer's disease. *Am. J. Pathol.* **153**, 1551-1560.

Kinoshita, M., Field, C. M., Coughlin, M. L., Straight, A. F. and Mitchison, T. J. (2002). Self- and actin-templated assembly of Mammalian septins. *Dev. Cell* **3**, 791-802.

Kramer-Zucker, A. G., Olale, F., Haycraft, C. J., Yoder, B. K., Schier, A. F. and Drummond, I. A. (2005a). Cilia-driven fluid flow in the zebrafish pronephros, brain and Kupffer's vesicle is required for normal organogenesis. *Development* **132**, 1907-1921.

Kramer-Zucker, A. G., Wiessner, S., Jensen, A. M. and Drummond, I. A. (2005b). Organization of the pronephric filtration apparatus in zebrafish requires Nephrin, Podocin and the FERM domain protein Mosaic eyes. *Dev. Biol.* **285**, 316-329.

Long, S., Ahmad, N. and Rebagliati, M. (2003). The zebrafish nodal-related gene southpaw is required for visceral and diencephalic left-right asymmetry. *Development* **130**, 2303-2316.

Mitchell, B., Jacobs, R., Li, J., Chien, S. and Kintner, C. (2007). A positive feedback mechanism governs the polarity and motion of motile cilia. *Nature* **447**, 97-101.

Mitra, S., Lukianov, S., Ruiz, W. G., Cianciolo Cosentino, C., Sanker, S., Traub, L. M., Hukriede, N. A. and Apodaca, G. (2012). Requirement for a uroplakin 3a-like protein in the development of zebrafish pronephric tubule epithelial cell function, morphogenesis, and polarity. *PLoS ONE* **7**, e41816.

Montagna, C., Lyu, M.-S., Hunter, K., Lukes, L., Lowther, W., Reppert, T., Hissong, B., Weaver, Z. and Ried, T. (2003). The Septin 9 (*MSF*) gene is amplified and overexpressed in mouse mammary gland adenocarcinomas and human breast cancer cell lines. *Cancer Res.* **63**, 2179-2187.

Moritz, O. L., Tam, B. M., Hurd, L. L., Peränen, J., Deretic, D. and Papermaster, D. S. (2001). Mutant rab8 Impairs docking and fusion of rhodopsin-bearing post-Golgi membranes and causes cell death of transgenic Xenopus rods. *Mol. Biol. Cell* **12**, 2341-2351.

Nachury, M. V., Loktev, A. V., Zhang, Q., Westlake, C. J., Peränen, J., Merdes, A., Slusarski, D. C., Scheller, R. H., Bazan, J. F., Sheffield, V. C. et al. (2007). A core complex of BBS proteins cooperates with the GTPase Rab8 to promote ciliary membrane biogenesis. *Cell* **129**, 1201-1213.

Nagata, K., Asano, T., Nozawa, Y. and Inagaki, M. (2004). Biochemical and cell biological analyses of a mammalian septin complex, Sept7/9b/11. *J. Biol. Chem.* **279**, 55895-55904.

Nauli, S. M., Alenghat, F. J., Luo, Y., Williams, E., Vassilev, P., Li, X., Elia, A. E. H., Lu, W., Brown, E. M., Quinn, S. J. et al. (2003). Polycystins 1 and 2 mediate mechanosensation in the primary cilium of kidney cells. *Nat. Genet.* **33**, 129-137.

Obara, T., Mangos, S., Liu, Y., Zhao, J., Wiessner, S., Kramer-Zucker, A. G., Olale, F., Schier, A. F. and Drummond, I. A. (2006). Polycystin-2 immunolocalization and function in zebrafish. *J. Am. Soc. Nephrol.* **17**, 2706-2718.

Pan, J., You, Y., Huang, T. and Brody, S. L. (2007). RhoA-mediated apical actin enrichment is required for ciliogenesis and promoted by Foxj1. *J. Cell Sci.* **120**, 1868-1876.

Park, T. J., Haigo, S. L. and Wallingford, J. B. (2006). Ciliogenesis defects in embryos lacking inturned or fuzzy function are associated with failure of planar cell polarity and Hedgehog signaling. *Nat. Genet.* **38**, 303-311.

Park, T. J., Mitchell, B. J., Abitua, P. B., Kintner, C. and Wallingford, J. B. (2008). Dishevelled controls apical docking and planar polarization of basal bodies in ciliated epithelial cells. *Nat. Genet.* **40**, 871-879.

Perner, B., Englert, C. and Bollig, F. (2007). The Wilms tumor genes *wt1a* and *wt1b* control different steps during formation of the zebrafish pronephros. *Dev. Biol.* **309**, 87-96.

Peterson, E. A., Kalikin, L. M., Steels, J. D., Estey, M. P., Trimble, W. S. and Petty, E. M. (2007). Characterization of a SEPT9 interacting protein, SEPT14, a novel testis-specific septin. *Mamm. Genome* **18**, 796-807.

Ravanelli, A. M. and Klingensmith, J. (2011). The actin nucleator Cordon-bleu is required for development of motile cilia in zebrafish. *Dev. Biol.* **350**, 101-111.

Robu, M. E., Larson, J. D., Nasevicius, A., Beiraghi, S., Brenner, C., Farber, S. A. and Ekker, S. C. (2007). p53 activation by knockdown technologies. *PLoS Genet.* **3**, e78.

Rothschild, S. C., Francescatto, L., Drummond, I. A. and Tombes, R. M. (2011). CaMK-II is a PKD2 target that promotes pronephric kidney development and stabilizes cilia. *Development* **138**, 3387-3397.

Sakamoto, T., Uezu, A., Kawauchi, S., Kuramoto, T., Makino, K., Umeda, K., Araki, N., Baba, H. and Nakanishi, H. (2008). Mass spectrometric analysis of microtubule co-sedimented proteins from rat brain. *Genes Cells* **13**, 295-312.

Shih, N.-Y., Li, J., Karpitskii, V., Nguyen, A., Dustin, M. L., Kanagawa, O., Miner, J. H. and Shaw, A. S. (1999). Congenital nephrotic syndrome in mice lacking CD2-associated protein. *Science* **286**, 312-315.

Sirajuddin, M., Farkasovsky, M., Hauer, F., Kühlmann, D., Macara, I. G., Weyand, M., Stark, H. and Wittinghofer, A. (2007). Structural insight into filament formation by mammalian septins. *Nature* **449**, 311-315.

Spiliotis, E. T., Kinoshita, M. and Nelson, W. J. (2005). A mitotic septin scaffold required for Mammalian chromosome congression and segregation. *Science* **307**, 1781-1785.

Spiliotis, E. T., Hunt, S. J., Hu, Q., Kinoshita, M. and Nelson, W. J. (2008). Epithelial polarity requires septin coupling of vesicle transport to polyglutamylated microtubules. *J. Cell Biol.* **180**, 295-303.

Sullivan-Brown, J., Schottenfeld, J., Okabe, N., Hostetter, C. L., Serluca, F. C., Thiberge, S. Y. and Burdine, R. D. (2008). Zebrafish mutations affecting cilia motility share similar cystic phenotypes and suggest a mechanism of cyst formation that differs from *pkd2* morphants. *Dev. Biol.* **314**, 261-275.

Sun, Z., Amsterdam, A., Pazour, G. J., Cole, D. G., Miller, M. S. and Hopkins, N. (2004). A genetic screen in zebrafish identifies cilia genes as a principal cause of cystic kidney. *Development* **131**, 4085-4093.

Tada, T., Simonetta, A., Batterton, M., Kinoshita, M., Edbauer, D. and Sheng, M. (2007). Role of Septin cytoskeleton in spine morphogenesis and dendrite development in neurons. *Curr. Biol.* **17**, 1752-1758.

Tamm, S. and Tamm, S. L. (1988). Development of macrociliary cells in Beroë. I. Actin bundles and centriole migration. *J. Cell Sci.* **89**, 67-80.

Thisse, C. and Thisse, B. (2008). High-resolution *in situ* hybridization to whole-mount zebrafish embryos. *Nat. Protoc.* **3**, 59-69.

Wasik, A. A., Polianskyte-Prause, Z., Dong, M.-Q., Shaw, A. S., Yates, J. R., 3rd, Farquhar, M. G. and Lehtonen, S. (2012). Septin 7 forms a complex with CD2AP and nephrin and regulates glucose transporter trafficking. *Mol. Biol. Cell* **23**, 3370-3379.

Werner, M. E., Hwang, P., Huisman, F., Taborek, P., Yu, C. C. and Mitchell, B. J. (2011). Actin and microtubules drive differential aspects of planar cell polarity in multiciliated cells. *J. Cell Biol.* **195**, 19-26.

Westerfield, M. (2000). *The Zebrafish Book. A Guide for the Laboratory Use of Zebrafish (Danio rerio)*. Eugene, OR: University of Oregon Press.

Xie, Y., Vessey, J. P., Konecna, A., Dahm, R., Macchi, P. and Kiebler, M. A. (2007). The GTP-binding protein Septin 7 is critical for dendrite branching and dendritic-spine morphology. *Curr. Biol.* **17**, 1746-1751.

Yelon, D., Horne, S. A. and Stainier, D. Y. R. (1999). Restricted expression of cardiac myosin genes reveals regulated aspects of heart tube assembly in zebrafish. *Dev. Biol.* **214**, 23-37.

Yoshimura, S., Egerer, J., Fuchs, E., Haas, A. K. and Barr, F. A. (2007). Functional dissection of Rab GTPases involved in primary cilium formation. *J. Cell Biol.* **178**, 363-369.

Zhao, C. and Malicki, J. (2007). Genetic defects of pronephric cilia in zebrafish. *Mech. Dev.* **124**, 605-616.

Journal of Cell Science